Molecular Crystals and Liquid Crystals

ISSN: 1542-1406 (Print) 1563-5287 (Online) Journal homepage: https://www.tandfonline.com/loi/gmcl20

Magnetic properties and sensitized visible and NIR luminescence of Dy^{III} and Eu^{III} coordination polymers by energy transfer antenna ligands

Mustafa Burak Coban, Cagdas Kocak, Hulya Kara, Muhittin Aygun & Asma Amjad

To cite this article: Mustafa Burak Coban, Cagdas Kocak, Hulya Kara, Muhittin Aygun & Asma Amjad (2017) Magnetic properties and sensitized visible and NIR luminescence of Dy^{III} and Eu^{III} coordination polymers by energy transfer antenna ligands, Molecular Crystals and Liquid Crystals, 648:1, 202-215, DOI: 10.1080/15421406.2017.1280911

To link to this article: https://doi.org/10.1080/15421406.2017.1280911

MOLECULAR CRYSTALS AND LIQUID CRYSTALS
2017, VOL. 648, 202–215
https://doi.org/10.1080/15421406.2017.1280911

Taylor & Francis
Taylor & Francis Group

Magnetic properties and sensitized visible and NIR luminescence of Dy^{III} and Eu^{III} coordination polymers by energy transfer antenna ligands

Mustafa Burak Coban[a,b], Cagdas Kocak[c], Hulya Kara[b,c], Muhittin Aygun[d], and Asma Amjad[e]

[a]Center of Science and Technology App. and Research, Balikesir University, Balikesir, Turkey; [b]Department of Physics, Faculty of Science and Art, Balikesir University, Balikesir, Turkey; [c]Department of Physics, Molecular Nano-Materials Laboratory, Faculty of Science, Mugla Sitki Kocman University, Mugla, Turkey; [d]Dokuz Eylul Univ, Faculty of Arts & Sciences, Department of Physics, Izmir, Turkey; [e]Dipartimento di Chimica "U. Schiff" and UdR INSTM, Università di Firenze, Sesto Fiorentino (FI), Italy

ABSTRACT

Two coordination polymers, {[Ln(2-stp)(4,4′-bipy)(H_2O)].(H_2O)}, [Ln = Dy (**1**) and Eu (**2**), 2-stp = 2-sulfoterephthalate and 4,4′-bipy = 4,4′-bipyridine] have been characterized by solid state UV-vis, FTIR spectra, X-ray single crystal diffraction and solid state photoluminescence. Variable-temperature magnetic susceptibility and isothermal magnetization as function of external magnetic field is also studied for both complexes. After ligand-mediated excitation, both complexes show the characteristic visible and NIR luminescence of the corresponding Ln^{III} ions (Ln = Dy, Eu) which is due to efficient energy transfer from the ligands to the central Ln^{III} ions *via* an antenna effect. The indirect energy transfer in both complexes has been investigated and discussed in detail.

KEYWORDS

Lanthanide; hydrothermal synthesis; photoluminescence, magnetism

Introduction

Investigation into the potential of lanthanide based complexes extending from understanding of fundamental concepts like quantum mechanical insight into quantum tunnelling of magnetization, coherence, luminescence, lighting, lasers, upconversion, and other unique photophysical properties, to their potential in applied science has taken an innovative turn in recent times [1]. Moreover, the structural diversity of lanthanide complexes with specifically designed ligands inspirited researchers to manipulate the resulting material properties to encompass and extend its application in more interdisciplinary areas like pharmaceutical studies [2]. As possible candidate for photoluminescence studies the lanthanide ions are known to showcase extremely narrow emission bands and intense long luminescence decay times (such as Eu^{III} and Tb^{III}) along with low absorption coefficients [3]. The poor absorption is the consequence of forbidden transitions on symmetry grounds between the 4f orbitals of the ions. The elucidation lies with the ligand-sensitized, near-infrared (NIR) luminescent

CONTACT Dr. Mustafa Burak Coban burakcoban@balikesir.edu.tr Center of Science and Technology App. and Research, Balikesir University, Balikesir, Turkey.
Color versions of one or more of the figures in the article can be found online at www.tandfonline.com/gmcl.

Ln^{III} complexes. Focus is provided in the design/choice of the sensitized ligands to promote population of the emitting levels of the ions followed by effective intramolecular energy transfer from the coordinated ligands to the central lanthanide ions, commonly known as the "antenna effect" [4]. Since the discovery of europium possessing light emission characteristics [5], the field has bloomed with efforts to optimize the choice of ligands with the lanthanide ions to enhance the luminescence properties and mitigation of energy to achieve higher efficiency.

2-Sulfoterephthalate (2-stp) ligand has two carboxylate groups and one sulfonate group, which show stronger coordination ability and more flexible coordination fashions as a linker and could be useful in construction of a new family coordination polymers. On the other hand, 4,4′-bipyridine (4,4′-bipy) ligand plays a key role in the construction of novel coordination polymers, for their abilities of coordinating to metal ions and altering the coordination environment of central ions and the dimension of the frame works. In order to obtain lanthanide-based coordination polymers, 2-sulfoterephthalate ligand has been used as versatile ligands [6,7]. Another effective approach for synthesis of coordination polymers is to incorporate a second organic ligand such as 4,4′-bipyridine into the structures [8,9].

Keeping the goals and problems in mind our group was motivated to identify new 4f-metal complexes designed with efficient antenna ligands to probe the sensitized visible and NIR luminescence. The crystal structures and photoluminescence properties in visible region of **1** and **2** were previously reported [10]. In order to elucidate the low temperature magnetic properties and NIR region photoluminescence properties of both compounds, we have synthesized the title compounds and re-determined their crystal structures. Herein, we report detailed solid state photoluminescence properties of both complexes and their free ligands (2-stp and 4,4′-bipy) in Visible and NIR region, and discussed indirect energy transfer mechanism *via* antenna effect. The IR and solid state UV-Vis spectra of **1** and **2** were analyzed in comparison with that of their free ligands (2-stp and 4,4′-bipy) and variable-temperature magnetic susceptibility and isothermal magnetization as function of external magnetic field is also studied for complexes **1** and **2**.

Experimental

Materials and physical measurements

All chemical reagents and solvents were purchased from TCI America or Aldrich and used without further purification. Elemental (C, H, N) analyses were carried out by standard methods with a LECO, CHNS–932 analyzer. FT-IR spectra were measured with a Perkin-Elmer Spectrum 65 instrument in the range of 4000–600 cm^{-1}. Powder X-ray measurements were performed using CuK_{α} radiation ($\lambda = 1.5418$ Å) on a Bruker-AXS D8-Advance diffractometer equipped with a secondary monochromator. The data were collected in the range $5° < 2\theta < 50°$ in $\theta-\theta$ mode with a step time of ns (5 s < n < 10 s) and step width of 0.02°. Solid state UV-visible spectra were measured at room temperature with an Ocean Optics Maya 2000Pro Spectrophotometer. Solid state photoluminescence spectra in the visible and NIR region were measured at room temperature with an ANDOR SR500i-BL Photoluminescence Spectrometer, equipped with a triple grating and an air-cooled CCD camera as detector. The measurements were done using the excitation source (349 nm) of a Spectra-physics Nd:YLF laser with a 5 ns pulse width and 1.3 mJ of energy per pulse as the source. DC Magnetic measurements were performed using a Quantum Design SQUID magnetometer with applied field of 0.1 T, except when otherwise stated. To avoid possible orientation effects, microcrystalline

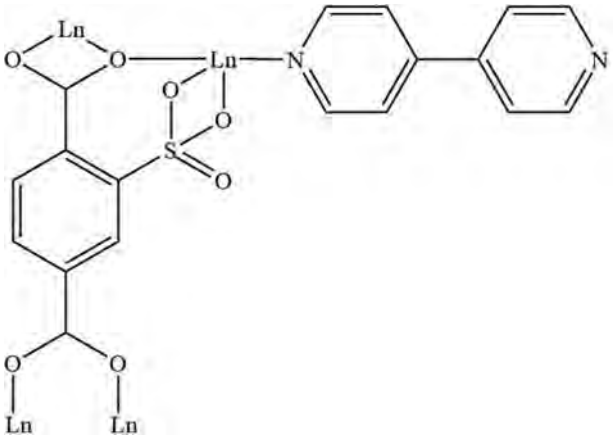

Scheme 1. A schematic representation of the compounds Ln = Dy (**1**) and Eu (**2**).

powders were pressed in pellets. The data were corrected for sample holder contribution and diamagnetism of the sample using Pascal constants.

Synthesis of [Dy(2-stp)(4,4′-bipy)(H_2O)].(H_2O) (1)

A mixture of $Dy(NO_3)_3.x(H_2O)$ (0.1 mmol), 2-NaH_2stp (0.1 mmol) and 4,4′-bipy (0.1 mmol) in 10 ml of distilled water was sealed into a bomb equipped with a Teflon liner (23 mL) and then heated at 140 °C for 5 days. The final pH values of these reactions media are close to 4.0. Crystals of Dy (**1**) (Orange) was collected and washed with distilled water (63% yield based on Dy). Elemental Analysis. $C_{18}H_{15}DyN_2O_9S$: Calcd. C, 28.45; H, 4.38; N, 3.69%; Found: C, 28.49; H, 4.32; N, 3.66%. IR: 3543, 2989, 2902, 1610, 1393, 1151, 851, 771, 620.

Synthesis of [Eu(2-stp)(4,4′-bipy)(H_2O)].(H_2O) (2)

A mixture of $Eu(NO_3)_3.5(H_2O)$ (0.1 mmol), 2-NaH_2stp (0.1 mmol) and 4,4′-bipy (0.1 mmol) in 10 ml of distilled water was sealed into a bomb equipped with a Teflon liner (23 mL) and then heated at 140 °C for 5 days. The final pH values of these reactions media are close to 4.0. Crystals of Eu (**2**) (Orange) was collected and washed with distilled water (62% yield based on Eu). A schematic representation of the compounds Ln = Dy (**1**) and Eu (**2**) are shown in Scheme 1. Elemental analysis. $C_{18}H_{15}EuN_2O_9S$: Calcd. C, 28.85; H, 4.44; N, 3.74%; Found: C, 28.81; H, 4.48; N, 3.72%. IR: 3549, 2987, 2901, 1610, 1393, 1153, 848, 770, 619.

X–ray structure determination

X-ray diffraction data of the complexes **1** and **2** were collected on a Xcalibur, Eos diffractometer using MoK_α radiation at room temperature (293 K). The data were corrected for Lorentz, polarization and absorption effects using the analytical numeric absorption correction technique [11]. Using Olex2 [12], all structures were solved by direct methods using SHELXS [13] and refined by full-matrix least-squares based on $|F_{obs}|^2$ using SHELXL [13]. The non-hydrogen atoms were refined anisotropically, while the hydrogen atoms, generated using idealized geometry, were made to "ride" on their parent atoms and used in the structure factor calculations. Details of the supramolecular π-interactions were calculated with PLATON 1.17 [14] program. ‡ CCDC–1451792 (**1**) and CCDC– 1451793 (**2**) contain the supplementary crystallographic data for **1** and **2**, respectively.

Result and discussion

X–ray structure of {[Ln(2-stp)(4,4′-bipy)(H_2O)].(H_2O)}, [Ln = Dy (1), and Eu (2)]

The crystal and molecular structures of **1** and **2**, previously described by Ren et al [10] was re-determined by us. Compounds **1** and **2** are isostructural. The Ln^{III} center are nine coordinated with seven oxygen atoms from four 2-stp ligands, one nitrogen atom from 4,4′-bipy ligand and one oxygen atoms from lattice water molecule (Fig. 1). The bond lengths and angles are similar to those already published. Further structural details are contained in SI and ref 10.

Compounds **1** and 2 are isostructural, hence only the structure of Dy (**1**) will be discussed in detail as a representative. The asymmetric unit of Dy (**1**) consists of one Dy^{III} ion, one 2-stp ligand, one 4,4′-bipy ligand, one coordinated and one lattice water molecule. The coordination environment of the Dy^{III} ion is shown in Fig. 1(a). Each Dy^{III} ion is nine coordinated, in which seven oxygen atoms from four 2-stp ligands with Dy–O bond distances in the range of 2.304(3)–2.572(3) Å and one nitrogen atom from 4,4′-bipy ligand with Dy–N bond length of 2.579(4) Å, and one oxygen atom from coordinated water molecule with Dy1–O1 = 2.344(3) Å (Fig. 1(a)). All bond distances and angles are comparable to similar structures [43, 46, 49, 50].

Dy1 and Dy1i are bridged through four 2-stp ligands in four directions to form a central symmetrically dimeric building unit, and the distance between the Dy^{III} ions in the dimeric unit is 3.9106 Å. Four 2-stp ligands in four directions bridge these dimer units and extend into two-dimensional (2D) (4,4) grid-like network (Fig. 2a). The 2-stp ligand adopts a hexadentate coordination mode (see Scheme 1) to connect four Dy^{III} ions to form a 2D framework. The intermolecular Dy^{III}–Dy^{III} distances are 10.052 Å and 11.514 Å in 2D framework (Fig. 2(b)).

Additional, 2D layers are connected by O–H···O and O–H···N hydrogen bonding network which leads to a three-dimensional (3D) structure for Dy (**1**) (Fig. 3(a)). It is interesting to note that different layered structure is also observed in the *bc*-plane, stacked orthogonally to the *a*-axis (Fig. 3(b)). This structures further stabilized by $\pi\cdots\pi$ stacking interactions (Table S3 and Fig. S1).

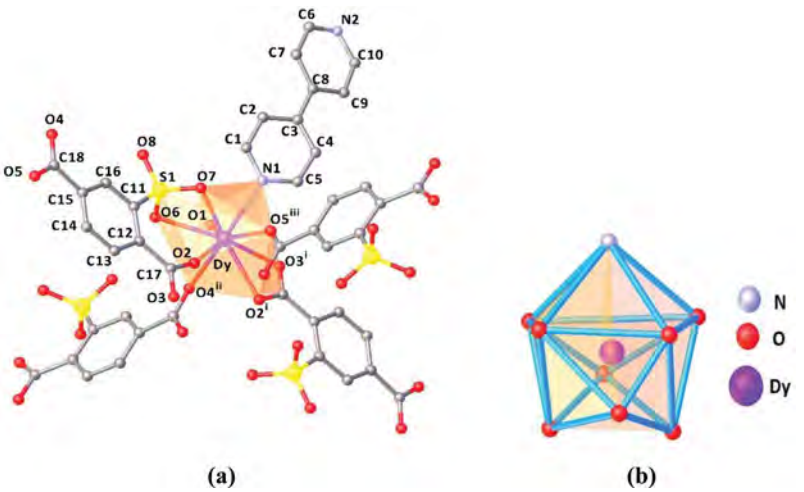

Figure 1. (a) Coordination environment of Dy^{III}. Lattice water molecule and hydrogen atoms are omitted for clarity. Displacement ellipsoids are drawn at the 50% probability level (Symmetry operation: i = 1-x,-y,2-z, ii = 1/2+x,1/2-y,1/2+z, iii = 1/2-x, -1/2+y, 3/2-z). (b) Distorted monocapped square-antiprism geometry surrounding the Dy^{III} atom in **1**.

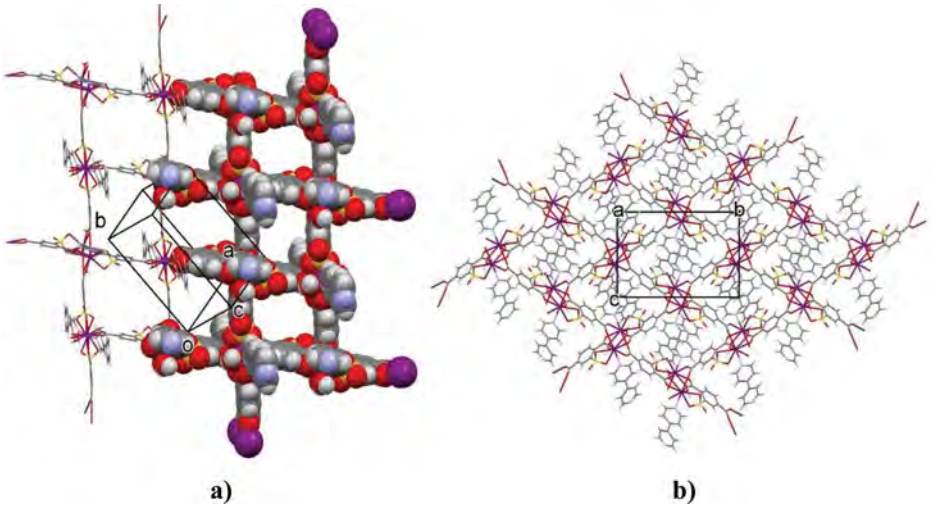

Figure 2. (a) The (4,4) grid-like network based on the dimer units and 2-stp ligands in the Dy (**1**). Lattice water molecules are omitted for clarity. (b) A 3D structure in the *bc*-plane of Dy (**1**).

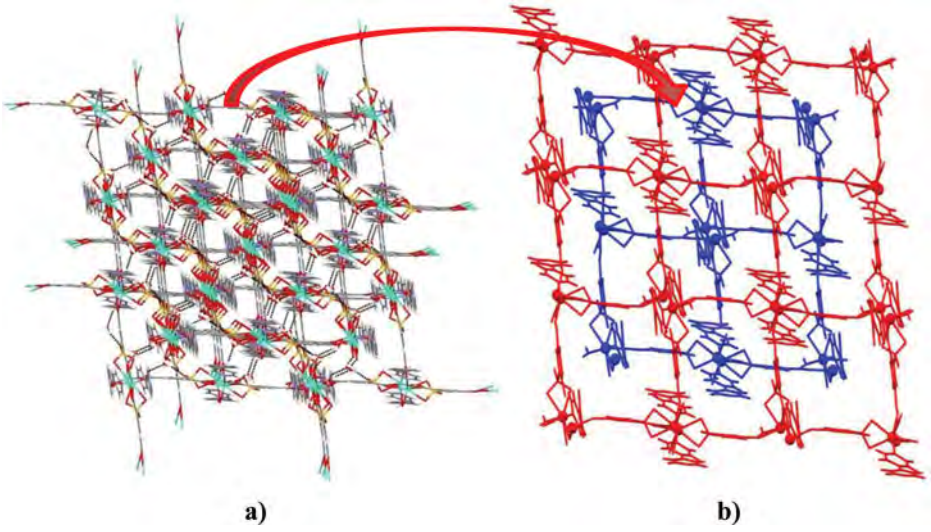

Figure 3. (a) Hydrogen bonded 3D structure and (b) its simplified network topology of Dy(**1**).

Finally, before proceeding to the spectroscopic, photoluminescence and magnetic characterization, we note that X-ray powder patterns for bulk microcrystalline samples of **1** and **2** were consistent with the exclusive presence of the phase identified in the single crystal experiment (Fig. S2).

FT-IR spectra

The IR spectra of **1** and **2** were analyzed in comparison with that of their free ligands (2-stp and 4,4′-bipy) which are in agreement with their single crystal structure analysis (Fig. 4). The broad bands at about 3543 cm^{-1} indicates the presence of ν(O-H) stretching frequency of coordinated water molecules. The strong absorption bands at 1390–1610 cm^{-1} and 1003–1292 cm^{-1} for both complexes are characteristic of the carboxylate group and the sulfonate

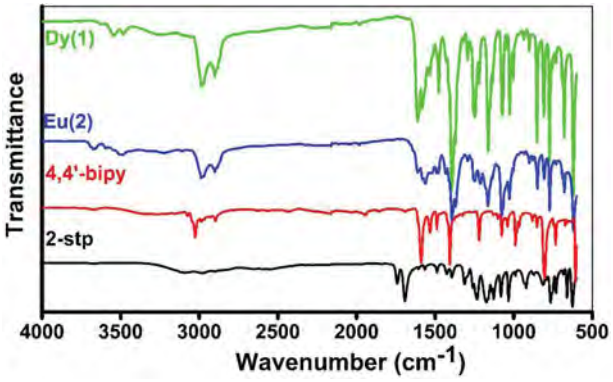

Figure 4. IR spectra for compound Dy (**1**), Eu (**2**), free 2-stp, and 4,4′-bipy ligands.

groups from 2-stp ligand, respectively [15,16]. The absorption peaks at around 606–880 cm^{-1} for **1** and **2**, which is conformity the absorption peaks of 4,4′-bipy ligand, may be attributed to the existence of coordinated 4,4′-bipy ligand [8,17].

Solid state UV-Vis Spectra

The solid state UV-Vis spectra of **1** and **2** were analyzed in comparison with that of their free ligands (2-stp and 4,4′-bipy) (Fig. 5). The absorption bands maxima at 375 nm for 2-stp and, 280 and 483 nm for 4,4′-bipy ligands, respectively. The absorption band at 280 nm, which can be assigned to the singlet-singlet $\pi-\pi^*$ absorption of the pyridine ring, while other absorption bands at 375 and 483 nm arise probably from the n-π^* transition of the free ligands [18,19].

Photoluminescence properties

The solid-state luminescent properties of the free 2-stp and 4,4′-bipy ligands and complexes **1** and **2** were investigated at room temperature in the visible and NIR regions upon excitation

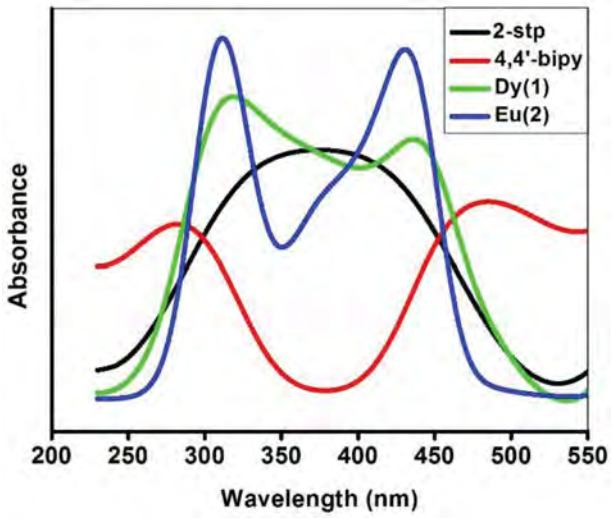

Figure 5. The absorption spectrum of the free 2-stp and 4,4′-bipy ligands and compounds **1** and **2**.

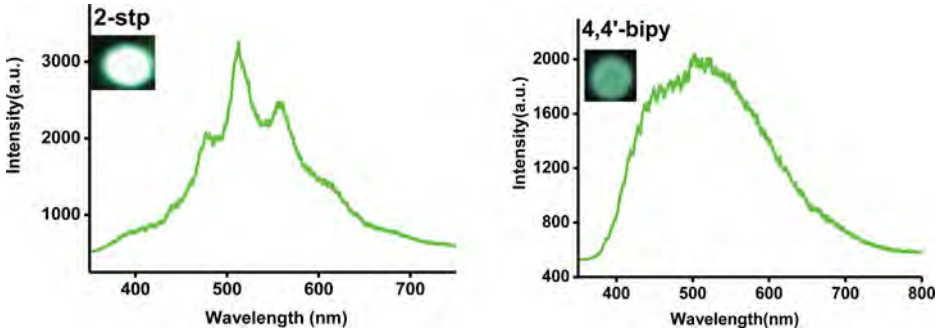

Figure 6. The emission spectrum of the free 2-stp (left) and 4,4′-bipy (right) ligands in solid samples at room temperature. ($\lambda_{exc.} = 349$ nm).

at $\lambda_{ex} = 349$ nm (Figs. 6 and 7). The free 2-stp ligand shows broad emission band at $\lambda_{max} = 480$ nm, 510 nm, and 558 nm whereas the free 4,4′-bipy ligand shows a broad emission band at $\lambda_{max} = 500$ nm which may be assigned to the $n \rightarrow \pi^*$ or $\pi \rightarrow \pi^*$ electron transition intra-ligand charge transfer (ILCT) [20]. To the best of our knowledge, photoluminescence properties of Dy^{III} compounds have rarely been reported in the NIR region so far [21, 22]. Compound Dy (**1**) displays intense typical yellow emission of the Dy^{III} ion (Fig. 7(a)). Four characteristic peaks are observed at 484 nm ($^4F_{9/2} \rightarrow {}^6H_{15/2}$), 573 nm ($^4F_{9/2} \rightarrow {}^6H_{13/2}$), 667 nm ($^4F_{9/2} \rightarrow {}^6H_{11/2}$) and 750 nm ($^4F_{9/2} \rightarrow {}^6H_{9/2} + {}^6F_{11/2}$) [23–26]. The characteristic yellow emission of $^4F_{9/2} \rightarrow {}^6H_{13/2}$ transition is much stronger than the blue emission of $^4F_{9/2} \rightarrow {}^6H_{15/2}$, so the Dy (**1**) compound emits yellow light [24]. Additionally, one weak characteristic peak is obtained at 840 nm correspond to $^4F_{9/2} \rightarrow {}^6H_{7/2}$ transition in the NIR region. For Eu (**2**), typical red emission of the Eu^{III} is detected and five characteristic peaks appearing at 579, 591, 613, 652 and 695 nm correspond to $^5D_0 \rightarrow {}^7F_j$ (j = 0-4) of Eu^{III} ions [24, 27]. Three weak characteristic emission peaks are also observed at 1160 nm, 1205 nm and 1370 nm correspond to $^7F_j \rightarrow {}^7F_0$ (j = 6-4) transitions in the NIR region (Fig. 7(b)). It is well known that the electric dipole $^5D_0 \rightarrow {}^7F_2$ transition is the most intense emission which leads to bright red luminescence and very sensitive to site symmetry, while the $^5D_0 \rightarrow {}^7F_1$ transition is magnetic-dipole and insensitive to site symmetry [24, 27, 28]. The intensity ratio I ($^5D_0 \rightarrow {}^7F_2$) / I ($^5D_0 \rightarrow {}^7F_1$) is equal to

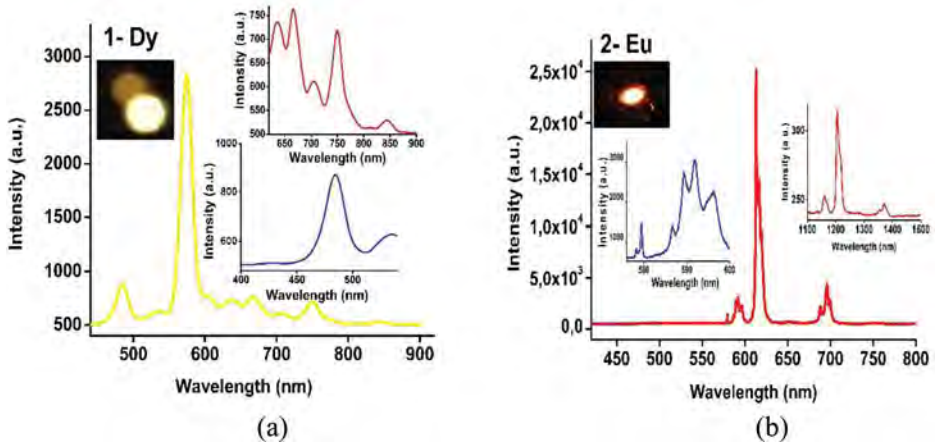

Figure 7. Room temperature solid-state photoluminescence spectrum of **1** and **2** ($\lambda_{exc} = 349$ nm). (a) Dy (**1**) (inset: (upper) the corresponding emission spectra in the region 650–900 nm, (below) an enlarged view of the emission spectrum in the region 400–525 nm), (b) Eu (**2**) (inset: (left) an enlarged view of the emission spectrum in the region 560–600 nm and (right) the corresponding emission spectra in the NIR region).

ca. 8, indicating that the Eu^{III} ions do not occupy inversion centers which is further confirmed by crystal structural analysis [28].

The lanthanide-based materials can generate a narrow strong emission bands due to f–f transitions originating from the emitting state of the Ln^{III} ion but the organic chromophores show the broad emission bands. The fact that emission bands of the free ligands do not appear in the emission spectra of compounds **1** and **2** proves that the free ligands act as strong sensitizer, efficiently transferring the excitation energy from ligands to the lanthanide ions. It is also well known that the coordinated water can quench the emission of Ln^{III} ion, but Dy (**1**) and Eu (**2**) exhibits intense emission, which also may be accounted for by the sensitization of the ligands and the extensive π system of the polymer structures [29–32].

Energy-transfer mechanism

For the Lanthanide compounds, characterization by low absorption coefficient, and direct excitation is rarely efficient. In this sense, the optical transitions within the 4f subshells of lanthanide ions are parity forbidden [31]. The lanthanide compounds strongly absorb light in the UV region and transfer the energy from the resonance level of the triplet state of the ligand to the 4f resonance levels of the lanthanide ions *via* an antenna effect (Fig. 8), which can be seen in the spectrum as the overlaps between the excitation spectrum of the complex and the absorption spectra of its ligands [33, 34]. In the excitation spectra of Dy (**1**) and Eu (**2**) and the absorption spectra of the ligands (2-stp and 4,4′-bipy) are shown in Fig. 9. There are overlaps between the excitation band of lanthanide [Ln = Dy (**1**) and Eu (**2**)] complexes and the absorption bands of the ligands [2-stp and 4,4′-bipy], which indicate that the typical sensitization of the Ln^{III} [Ln = Dy (**1**) and Eu (**2**)] ions by the both ligands a *via* an "antenna effect." Furthermore, the overlap of wavelength range between the absorption band of 2-stp and the excitation band of Ln^{III} [Ln = Dy (**1**) and Eu (**2**)] complexes are bigger than that of 4,4′-bipy, which suggests that the antenna effect of the 2-stp ligand is more efficient sensitizer than 4,4′-bipy. As a result, the intramolecular energy transfer in Dy (**1**) and Eu (**2**) complexes mostly happen between the 2-stp ligand and the Dy^{III} or Eu^{III} ions [34].

Energy transfer pathway for the sensitization of Ln^{III} ion photoluminescence is mostly the ligand-to-metal energy transfer from the lowest triplet level of ligand to an excited state of lanthanide ion through a non-radiative transition [19]. In terms of Scheme 2; the sensitization steps take place: (i) the ligands absorb the energy and are excited to do singlet (S_1) excited state, (ii) The energy of (S_1) excited state is then transferred to the triplet excited state (T) of

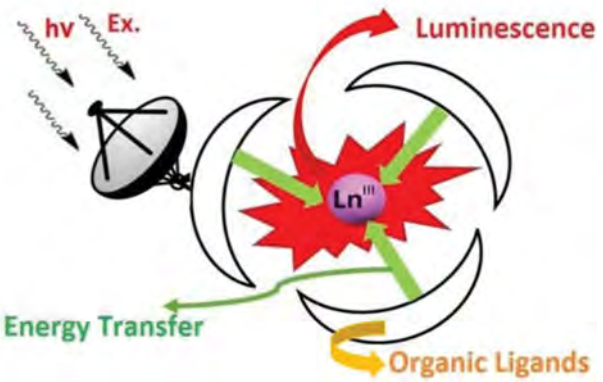

Figure 8. Sensitization of the intra-4f transition of Ln^{III} by organic ligands "antenna."

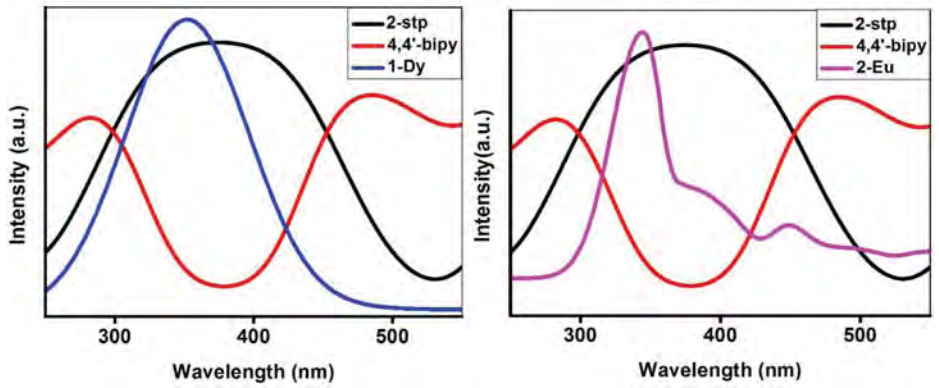

Figure 9. Excitation spectrum for Dy (**1**) (left) and Eu (**2**) (right), absorption spectrum of the free 2-stp and 4,4′-bipy ligands as solid state.

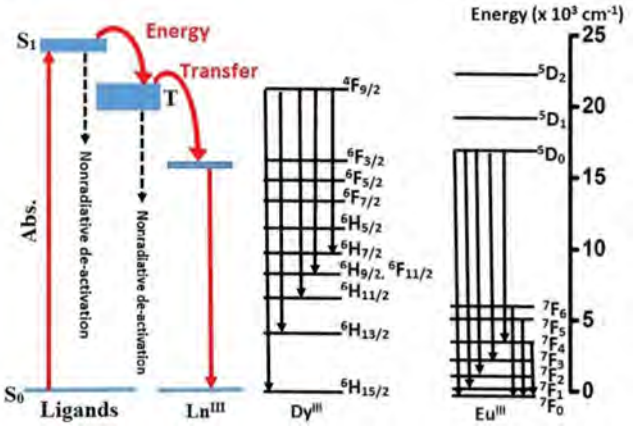

Scheme 2. The energy transfer mechanism (left) and energy level diagrams of Dy^{III} and Eu^{III} ions (right).

the ligands through intersystem crossing (ISC) [35], (iii) the energy is transferred to the 4f levels of the Ln^{III} ions, resulting in the emission of the sensitized Ln^{III} ions [25]. According to the Dexter's theory, the energy gap between the 4f levels of the lanthanide ions and the resonance level of the triplet state of the ligand should be matched. If the energy gap is too big, the overlap between the ligand and the Ln^{III} ion will decrease, and finally the energy transfer rate constant would reduce sharply. On the contrary, if the energy gap is too small, there will be an energy back-transfer from the Ln^{III} ions to the resonance level of the triplet state of the ligand [36]. In our case, the triplet-state energy level of 2-stp and 4,4′-bipy ligands were measured and calculated to be 20,900 and 20,000 cm^{-1}, respectively. These values match well with the 4f levels Dy^{III} and Eu^{III} ions, which are ideal for efficient energy transfer from the ligands to the corresponding lanthanide ions [31].

Magnetic properties of 1 and 2

Magnetic susceptibility measurements were performed on polycrystalline samples of Dy (**1**) and Eu (**2**), respectively, in the 2−40 K temperature range with an applied Dc field of 1 KOe and in the 40−300 K temperature range with an applied Dc field of 10 KOe (Figs. 10 and 12). At room temperature, the $\chi_M T$ value is 14.22 cm^3 K mol^{-1} for Dy (**1**). These value is close to

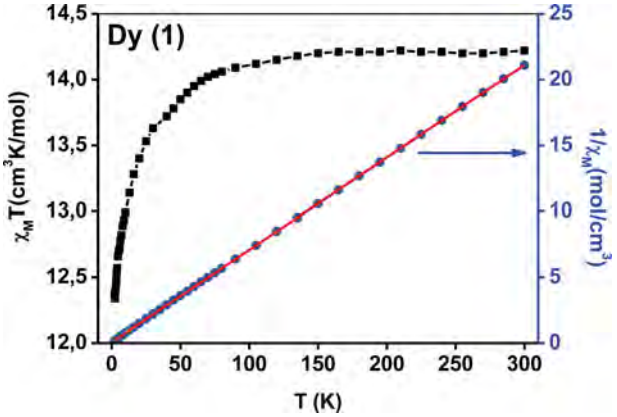

Figure 10. Temperature dependence of $\chi_M T$ vs T and $\chi_M{}^{-1}$ versus T for Dy (**1**). The solid red line represents the best fit using Curie-Weiss law.

those expected for an isolated Ln^{III} ions; Dy^{III}: 14.17 cm^3 K mol^{-1} ($S = 5/2$, $L = 5$, $^6H_{15/2}$, $g_J = 4/3$). Upon cooling, the $\chi_M T$ value decreases gradually to reach a minimal value of 12.37 cm^3 K mol^{-1} for Dy (**1**) at 2 K. The decrease in $\chi_M T$ product upon lowering the temperature can be accredited to three factors: (i) antiferromagnetic interactions between the Ln^{III} ions, (ii) the thermal depopulation of Stark sublevels together with crystal-field affection, and (iii) the presence of significant magnetic anisotropy of the Ln^{III} ions. Due to the presence of all these combined effects in these complexes, it is difficult to separately quantify each contribution [37–39]. As a complementary characterization, the field dependence of magnetization for Dy (**1**) has been measured at 2.0 K (Fig. 11). The magnetization increases rapidly at low field and eventually reaches saturation of 8.89 $N\mu_B$ at 5 T which is smaller than the theoretical value ($g_J J = 4/3 \times 15/2 = 10\ N\mu_B$) for each Dy^{III} ion. Non-saturation of the magnetization indicates the presence of significant magnetic anisotropy and/or low-lying excited states for Dy (**1**).

The theoretical treatment of the data is enforced using the Curie-Weiss law to probe semi-quantitatively the magnitude of the exchange constant J_{EX} and the Van Vleck expression that further encompasses the crystal filed effects expected in the semi integral spin systems. For Dy (**1**), the crystal field is expected to have a more profound effect on the $\chi_M T$ vs T behavior. Due to low symmetry of the said complex, one would have to determine 27 crystal field parameters. So, to avoid over parameterization, a single crystal field splitting parameter D is used in the

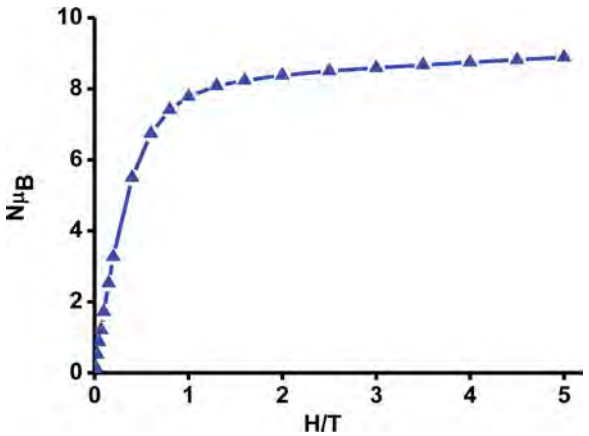

Figure 11. Field dependence of magnetization of Dy (**1**) at 2 K.

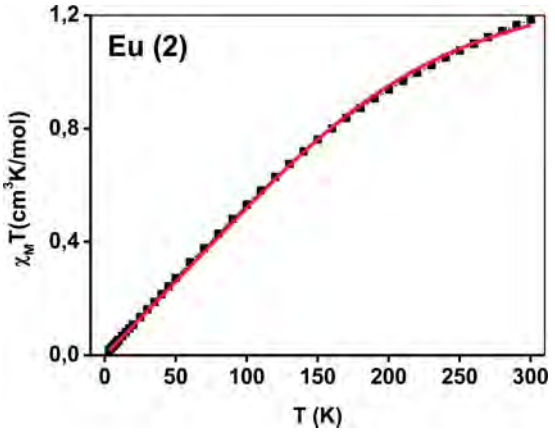

Figure 12. The plot of $\chi_M T$ versus T for Eu (**2**). The solid red lines represent the best-fit using Eq. (1) for Eu (**2**).

analysis. This is equivalent to assuming that splitting of the $J = 15/2$ ground state may occur into $2J+1$ levels due to an axial, second order crystal field. However, a reliable fit was not achieved, leading to the fact that an extensive ab initio guesses of CF parameters is required, which is currently point beyond the scope of this work. Furthermore, using Curie-Weiss and $\theta = \frac{zJ_{EX}J(J+1)}{3k}$, J_{EX} was extrapolated for Dy (**1**), where z is the number of nearest neighbors, 1 in our case and k is the Boltzmann constant. In all cases θ is found to be negative, i.e., a negative exchange coupling parameter J_{EX}, further confirming the existence of weak antiferromagnetic interactions in the system. The best least-squares fit of the experimental magnetic data from the Curie Weiss law is $\theta = -0.148 \pm 0.011$, J_{EX} =-0.005 cm^{-1} and $C = 13.053 \pm 0.047$.

On the other hand, Eu (**2**) is analyzed with a different approach, a consequence of thermally populated excited multiplets in such ion. The spin-orbit coupling in the system instigate the splitting of the ground term $^7F_0$ for Eu^{III}, resulting in an energy separation from the ground state that can be equal to k_BT at room temperature [40]. As can be seen from Fig. 12, the $\chi_M T$ value is nearly linear over the whole temperature range for Eu (**2**). The $\chi_M T$ values at room temperature are 1.18 cm^3 K mol^{-1} for Eu (**2**). This value is larger than the theoretical values of 0.0 cm^3 mol^{-1} K for one isolated Eu^{III} ion ($S = 3$, $L = 3$, $^7F_0$, $g = 5$) in the ground state. Because not only the ground state of this metal ion but also the first [$^7F_1$ for Eu^{III}] and even highly exited states can be populated at room temperature [41], which bring about magnetic properties deviating from the Curie-Weiss (Fig. S3). The $\chi_M T$ values of this compound decrease monotonically with cooling temperature to a value of 0.017 cm^3 mol^{-1} K for Eu (**2**) at 3 K, which indicate the depopulation of the excited states. Since the ground state is non-magnetic, the crystal field effects are ignored and the magnetic susceptibilities can be fitted with a single-ion Eu^{III} model based on eq. (**1**) [42] which only considers the spin–orbital coupling of Eu^{III} ions:

$$\chi_M T_{Eu} = \left(\frac{N\beta^2}{3kx}\right)\left[24 + \left(\frac{27x}{2} - \frac{3}{2}\right)e^{-x} + \left(135x - 2 - \frac{5}{2}\right)e^{-3x} + \left(189x - \frac{7}{2}\right)e^{-6x} + \left(405x - \frac{9}{2}\right)e^{-10x} + \left(\frac{1485x}{2} - \frac{11}{2}\right)e^{-15x} + \left(\frac{2457x}{2} - \frac{13}{2}\right)e^{-21x}\right] \Big/ \times\left[1 + 3e^{-x} + 5e^{-3x} + 7e^{-6x} + 9e^{-10x} + 11e^{-15x} + 13e^{-21x}\right]$$

$$x = \lambda/kT \tag{1}$$

Table 1. Magnetic data for **1** and **2** and a series of related compounds.

Complex	Ln …Ln	C	θ	λ	g	Ref
Dy **(1)**	3.911	13.053	− 0.14			This work
Dy	3.768	14.17			4/3	[43]
Dy	3.912	13.48	− 2.24			[44]
Dy	4.182	14.30			4/3	[45]
Dy	4.125	14.17				[46]
Eu **(2)**	3.956		—	416		This work
Eu	3.949		− 1.14	349	—	[47]
Eu	4.4214		1.21	404	—	[41]
Eu	4.274			336	1.95	[42]
Eu	4.503			488	—	[48]

A reasonable fit is achieved with spin-orbit coupling $\lambda = 416.15 \pm 2.67$ cm^{-1}, with $R = 4.35 \times 10^{-4}$, as shown in Fig. 12. For Eu^{III} all the g_J factors are equal to 3/2, except g_0 which is 5 [40]. Despite λ being towards the higher end, similar values have already been reported (Table 1).

Conclusion

In this work we presented extensive optical and magnetic characterization of two coordination polymers with Dy (**1**) and Eu (**2**). The solid-state photoluminescence measurements display remarkable yellow emission for Dy (**1**) and red emission for Eu (**2**), which are attributed to the Ln^{III} f–f electronic transitions. In addition, these compounds indicate efficient energy transfer from ligand to metal ions, which is known as "antenna effect." The dc magnetic properties of the complexes were found to be in good agreement with the literature, and analysis of the data using Curie-Wiess for **1** and single–ion model considering only the spin–orbital coupling for **2** dictates antiferromagnetic coupling in the complexes. It is imperative to extend the study of NIR emission to other Ln^{III} complexes and sensitized ligands to achieve stable, accessible energy pathways to ensure the realization of these complexes as technological applications.

Funding

The authors are grateful to the Research Funds of Balikesir University (BAP-2015/128) and Mugla Sitki Kocman University (BAP-2017/035) for the financial support.

Acknowledgments

The authors thank Dokuz Eylul University for the use of the Agilent Xcalibur Eos diffractometer (purchased under University Research Grant No. 2010.KB.FEN.13) and Balikesir University, Science and Technology Application and Research Center (BUBTAM) for the use of the Photoluminescence Spectrometer. Asma Amjad would like to thank Ente CRF. The authors are also very grateful to Prof. Dr. Andrea Caneschi (Laboratory of Molecular Magnetism, Department of Chemistry, University of Florence) for the use of SQUID magnetometer and helpful suggestions.

References

[1] (a) Layfield, R. A., & Murugesu, M. (editors) (2015). *Lanthanides and actinides in molecular magnetism*, Verlag GmbH, Weinheim. (b) Wang, B. W., Jiang, S. D., Wang, X. T., & Gao, S. (2009). *Sci China Ser B-Chem.*, *52*(11), 1739–1758. (c) Yang, D., Wei, M. (editors) (2015). *Photofunctional*

layered materials, Structure and Bonding Springer International Publishing, Switzerland. (d) Patterson, A. R., Schmitt, W., & Evans, R. C. (2014). *J. Phys. Chem. C*, *118*, 10291–10301. (e) Cui, Y., Yue, Y., Qian, G., & Chen, B. (2012). *Chem. Rev.*, *112*, 1126–1162. (f) Kido, J., & Okamoto, Y. (2002). *Chem. Rev.*, *102*, 2357–2368. (g) El Halawany, A., He, S., Hodaei, H., Bakry, A., Razvi, M. A. N., Alshahrie, A., Johnson, N. J. J., Christodoulides, D. N., Almutairi, A., & Khajavikhan, M. (2016). *Optics Express*, *24*(13), 13999–14009. (h) Blasse, G., & Grabmaier, B. (1994). *Luminescent materials*, Springer: Berlin, Germany.

[2] (a) Mawani, Y. Y., Cawthray, J. F., Chang, S., Sachs-Barrable, K., Weekes, D. M., Wasan, K. M., & Orvig, C. (2013). *Dalton Trans.*, *42*(17), 5999–6011. (b) Rhule, J. T., Hill, C. L., & Judd, D. A. (1998). *Chem. Rev.*, *98*, 327–358.

[3] Sabbatini, N., Guardigli, M., & Lehn, J.-M. (1993). *Coord. Chem Rev.*, *123*, 201–228.

[4] Dong, H., Sun, L.-D., & Yan, C.-H. (2015). *Chem. Soc. Rev.*, *44*, 1608–1634.

[5] Weissman, S.I. (1942). *J. Chem Phys*, *10*, 214–217.

[6] Ren, Y., Ma, H., Fu, F., Zhang, Z., & Zhang, Y. (2013). *J. Inorg. Organomet. P.*, *23*, 646–651.

[7] Ren, Y.X., Jia, T.J., Li, L.C., & Zheng, X.J. (2013). *Z. Anorg. Allg. Chem.*, *639*, 928–933.

[8] Coban, M.B., Erkarslan, U., Oylumluoglu, G., Aygun, M., & Kara, H. (2016). *Inorg. Chim. Acta*, *447*, 87–91.

[9] Coban, M. B., Amjad, A., Aygun, M., & Kara, H. (2017). *Inorg. Chim. Acta*, *455*, 25–33.

[10] Ren, Y.-X., An, M., Chai, H.-M., Zhang, M.-L., & Wang, J.-J. (2015). *Z. Anorg. Allg. Chem.*, *641*(3–4), 525–528.

[11] Clark, J. S., & Reid, R.C. (1995). *Acta Crystallogr.*, *A51*, 887–897.

[12] Dolomanov, H., Bourhis, O.V., Gildea, L.J., Howard, R.J., & Puschmann, J.A.K. (2009). *J. Appl. Crystallogr.*, *42*, 339–341.

[13] Sheldrick, G.M. (2008). *Acta Crystallogr. A*, *64*, 112–122.

[14] Spek, A.L. (2009). *Acta Cryst.*, *D65*, 148–155.

[15] Liu, Q.Y., & Xu, L. (2005). *Eur. J. Inorg. Chem.*, *17*, 3458–3466.

[16] Xiao, H.-P., Zheng, Y.-X., Liang, X.-Q., Zuo, J.-L., & You, X.-Z. (2008). *J. Mol. Struct.*, *888*(1–3), 55–61.

[17] Mao, H., Zhang, C., & Shi, H. (2011). *J. Phys. Chem. Solids*, *72*(11), 1230–1238.

[18] Zhou, X., Zhao, X., Wang, Y., Wu, B., Shen, J., Li, L., & Li, Q. (2014). *Inorg. Chem.*, *53*, 12275–12282.

[19] Shen, H.-Y., Wang, W.-M., Gao, H.-L., & Cui, J.-Z. (2016). *RSC Adv.*, *6*(41), 34165–34174.

[20] Feng, X., Feng, Y.-Q., Chen, J. J., Ng, S.-W., Wang, L.-Y., & Guo, J.-Z. (2015). *Dalton Trans.*, *44*(2), 804–816.

[21] Maxim, C., Branzea, D. G., Tiseanu, C., Rouzieres, M., Clerac, R., Andruh, M., & Avarvari, N. (2014). *Inorg. Chem.*, *53*(5), 2708–2717.

[22] Ma, P., Wan, R., Si, Y., Hu, F., Wang, Y., Niu, J., & Wang, J. (2015). *Dalton Trans.*, *44*(25), 11514–11523.

[23] Wang, H.-S., Li, G.-C., Chen, Y., Zhang, Z.-J., & Liu, M.-L. (2010). *J. Coord. Chem.*, *63*(23), 4068–4076.

[24] Wu, Q.-R., Wang, J.-J., Hu, H.-M., Shangguan, Y.-Q., Fu, F., Yang, M.-L., Dong, F.-X., & Xue, G.-L. (2011). *Inorg. Chem. Commun.*, *14*(3), 484–488.

[25] Biju, S., Gopakumar, N., Scopelliti, R., Kim, H. K., & Reddy, M. L. P. (2013). *Inorg. Chem.*, *52*, 8750–8758.

[26] Wang, P., Fan, R.-Q., Yang, Y.-L., Liu, X.-R., Xiao, P., Li, X.-Y., Hasi, W., & Cao, W.-W. (2013). *CrystEngComm*, *15*(22), 4489–4056.

[27] Liu, C.-B., Li, Q., Wang, X., Che, G.-B., & Zhang, X.-J. (2014). *Inorg. Chem. Commun.*, *39*, 56–60.

[28] Li, H.-N., Li, H.-Y., Li, L.-K., Xu, L., Hou, K., Zang, S.-Q., & Mak, T. C. W. (2015). *Cryst. Growth Des.*, *15*(9), 4331–4340.

[29] Blasse, G., & Grabmaier, B. (1994). *Luminescent materials*, Springer: Berlin, Germany.

[30] Ahmed, Z., & Iftikhar, K. (2010). *Inorg. Chim. Acta*, *363*(11), 2606–2615.

[31] Dang, S., Yu, J., Wang, X., Sun, L., Deng, R., Feng, J., Fan, W., & Zhang, H. (2011). *J. Lumin.*, *131*(9), 1857–1863.

[32] Lyapin Ryabochkina, P., Chabushkin, A. N., Ushakov, S.N., & Fedorov, P.P. (2015). *J. Lumin.*, *167*, 120–125.

[33] Dang, S., Yu, J.B., Wang, X.F., Guo, Z. Y., Sun, L.N., Deng, R.P., Feng, J., Fan, W.Q., & Zhang, H.J. (2010). *J. Photochem. Photobio. A: Chem.*, *214*(2-3), 152–160.

[34] Dang, S., Sun, L., Zhang, H., Guo, X.-M., Li, Z., Feng, J., Guo, H.-D., & Guo, Z. (2008). *J. Phys. Chem. C*, *112*(34), 13240–13247.
[35] Sun, L., Qiu, Y., Liu, T., Zhang, J. Z., Dang, S., Feng, J., Wang, Z., Zhang, H., & Shi, L. (2013). *ACS Appl. Mater. Interfaces*. *5*(19), 9585–9593.
[36] Dang, S., Sun, L.-N.N., Song, S.-Y.Y., Zhang, H.-J.J., Zheng, G.-L.L., Bi, Y.-F. F., Guo, H.-D.D., Guo, Z.-Y.Y., & Feng, J. (2008). *Inorg. Chem. Commun.*, *11*(5), 531–534.
[37] Zhang, H.-B., Tian, C.-B., Wu, S.-T., Lin, J.-D., Li, Z.-H., & Du, S.-W. (2011). *J. Mol. Struct.*, *985*(2-3), 355–360.
[38] Beloborodov, S.S., Levchenkov, S.I., Popov, L.D., Lukov, V.V., Shcherbakov, I.N., Alexandrov, G.G., & Kogan, V.A. (2014). *Mendeleev Commun.*, *24*(4), 219–221.
[39] Savard, D., Lin, P.H., Burchell, T.J., Korobkov, I., Wernsdorfer, W., Clerac, R., & Murugesu, M. (2009). *Inorg. Chem.*, *48*(24), 11748–11754.
[40] Kahn, O. (1993). *Molecular magnetism*, Verlag, Weinheim, New York.
[41] Li, Y., Zheng, F., Liu, X., Zou, W., Guo, G., Lu, C., Huang, J.-S., & Academy, C. (2006). *Inorg. Chem.*, *45*(16), 6308–6316.
[42] Xu, N., Wang, C., Shi, W., Yan, S. P., Cheng, P., & Liao, D.Z. (2011). *Eur. J. Inorg. Chem.*, (15), 2387–2393.
[43] Long, J., Habib, F., Lin, P.H., Korobkov, I., Enright, G., Ungur, L., Wernsdorfer, W., Chibotaru, L.F., & Murugesu, M. (2011). *J. Am. Chem. Soc.*, *133*(14), 5319–5328.
[44] Tan, X., Che, Y., & Zheng, J. (2013). *Inorg. Chem. Commun.*, *35*, 231–234.
[45] Wei, X.-H., Yang, L.-Y., Liao, S.-Y., Zhang, M., Tian, J.-L., Du, P.-Y., Gu, W., & Liu, X. (2014). *Dalton Trans.*, *43*(15), 5793–5800.
[46] Zhang, H., Lin, S.-Y., Xue, S., Wang, C., & Tang, J. (2014). *Dalton Trans.*, *43*, 6262–6268.
[47] Ji, B., Deng, D., He, X., Liu, B., Miao, S., Ma, N., Wang, W., Ji, L., Liu, P., & Li, X. (2012). *Inorg. Chem.*, *51*(4), 2170–2177.
[48] Hou, Y.-L., Xiong, G., Shen, B., Zhao, B., Chen, Z., & Cui, J.-Z. (2013). *Dalton Trans.*, *42*(10), 3587–3596.
[49] Wu, G., Yin, F. J., Wei, H., Liu, Z. F., & Yin, G. (2011). *Z. Anorg. Allg. Chem.*, *637*(5), 602–607.
[50] Zhou, R.S., Ye, L., Ding, H., Song, J.F., Xu, X.Y., & Xu, J.Q. (2008). *J. Solid State Chem.*, *181*(3), 567–575.